Geophysical Research Letters

RESEARCH LETTER
10.1029/2020GL089346

Momentum and Energy Predict the Backwater Rise Generated by a Large Wood Jam

E. Follett[1], I. Schalko[2], and H. Nepf[2]

[1]School of Engineering, Cardiff University, Cardiff, UK, [2]Department of Civil and Environmental Engineering, Massachusetts Institute of Technology, Cambridge, MA, USA

Key Points:
- Logjams act as a porous obstruction, generating momentum loss described by an adaptation of the canopy drag model
- Backwater rise is predicted from unit discharge and a dimensionless parameter, found from jam structure or unit discharge and water depth
- Backwater length, pool size, and upstream sediment deposition depend on jam structure and channel slope

Supporting Information:
- Supporting Information S1

Correspondence to:
E. Follett,
emf@alum.mit.edu

Citation:
Follett, E., Schalko, I., & Nepf, H. (2020). Momentum and energy predict the backwater rise generated by a large wood jam. *Geophysical Research Letters*, *47*, e2020GL089346. https://doi.org/10.1029/2020GL089346

Received 16 JUN 2020
Accepted 10 AUG 2020
Accepted article online 17 AUG 2020

Abstract Wood reintroduction is now considered an important aspect of stream restoration, due to ecohydraulic benefits associated with wood presence. Channel-spanning wood jams create an upstream backwater, increasing flow heterogeneity, sediment deposition, and ecological productivity, but also flood risk. Backwater rise prediction is necessary to evaluate flood hazards in hydraulic models, improve design of engineered logjam projects, and compare jam effects across river systems. We present experimental results demonstrating that a jam can be modeled as a porous obstruction generating momentum loss proportional to the number, size, and packing density of the logs and the jam length. Energy and momentumconstraints are combined to predict backwater rise from unit discharge and a dimensionless structural parameter. This novel approach allows description of preexisting jams with a common metric. The model was used to demonstrate how backwater length, pool size, and upstream sediment deposition depend on jam structure and channel slope.

Plain Language Summary Logjams generate important riverine habitat by increasing the upstream water surface elevation, creating an upstream pool with slower, deepened water. Prediction of the change in upstream water surface elevation from the shape of logs and fine material (branches and leaves) within the jam and river discharge is necessary to understand a jam's contribution to geomorphic and ecological diversity, to improve design of restoration projects, and to estimate flood risk. Existing approaches either consider collections of individual logs, which cannot describe large jams, or are based only on empirical equations. Using 584 flume experiments, we demonstrate that jams composed of many logs act as a porous structure that generates momentum loss proportional to the number, size, and packing density of the logs and the length of the jam. Backwater rise is predicted from unit discharge, unobstructed water depth, anda dimensionless jam structural parameter. This structural parameter comprises log number, size, and packing density and can be found from a set of measurements of river discharge and water depth upstream and downstream of the jam. We further demonstrate how the length of the backwaterrise, associated pool size, and the increase of sediment deposition depend on jam structure and channel slope.

1. Introduction

The presence of large wood (LW, defined as logs with diameter ≥0.1 m and length ≥1.0 m, Keller & Swanson, 1979; Wohl & Jaeger, 2009) in river channels creates heterogeneous hydraulic conditions and increases channel-floodplain connectivity, leading to the formation of multiple channels and highly productive floodplain wetlands (Abbe & Montgomery, 2003; Bertoldi et al., 2015; Gippel, 1995; Keller & Swanson, 1979; Wallerstein et al., 2001; Wohl & Goode, 2008; Wohl et al., 2016). LW jams commonly form at natural and artificial obstructions and may include branches, needles, and leaves, defined as organic fine material *FM*. In addition to direct hydraulic impacts, LW jams provide overhead cover for fish and invertebrates and promote storage of fine sediment and organic matter (Beckman & Wohl, 2014; Dixon, 2016; Entrekin et al., 2008; Wohl et al., 2016).

Under some conditions, the backwater rise generated by LW jams poses a flood hazard (Comiti et al., 2016; Schmocker & Hager, 2013; Steeb et al., 2017; Wallerstein et al., 2001; Wohl et al., 2016). Recent floods demonstrated that the transported wood volume in rivers can significantly increase in extreme conditions (Bezzola & Hegg, 2007; Comiti et al., 2016; Steeb et al., 2017). Transported wood may block river infrastructure including bridges (De Cicco et al., 2017; Panici & de Almeida, 2018). Due to the increased flood risk, the amount of LW in rivers has been significantly reduced from historic levels through targeted LW removal

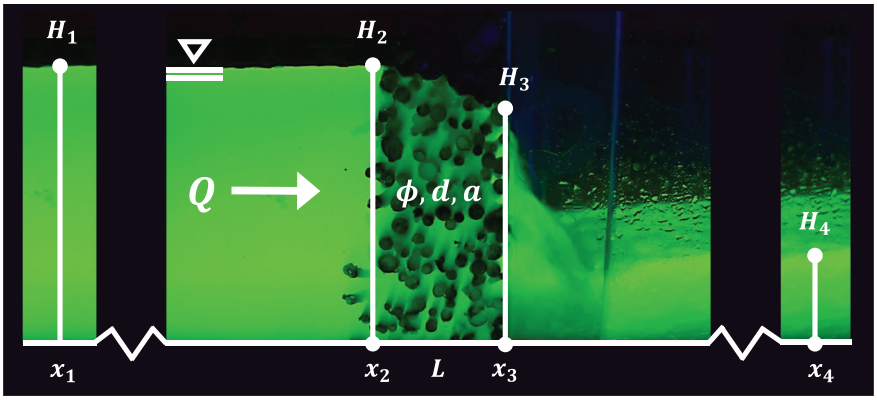

Figure 1. Side view of test setup with discharge Q ($m^3 s^{-1}$) flowing through channel-spanning jam with length L (m), solid volume fraction ϕ, LW diameter d (m), frontal area per jam volume a (m^{-1}), and flume width B (m). Cross-sections correspond to longitudinal distances x_1, x_2, x_3, x_4 (m) with water depth H_1, H_2, H_3, H_4 (m) measured relative to the channel bed. In all cases adjustment at x_2 had no observable effect on the water surface profile, so $H_1 \cong H_2$. Apparent curvature in water surface profile at point illustrating x_4 is due to photo parallax and was not present at the measurement point (1 m downstream of jam trailing edge).

campaigns as well as concurrent logging activity (Gurnell et al., 2018; Wohl, 2017). However, channel-spanning LW jams continue to play a significant role in forested areas (Dixon, 2016; Haschenburger & Rice, 2004; Wohl, 2017). For example, Dixon (2016) observed that 31% (16/51) of logjams on a 4.5 km stretch of a small forest stream in the Highland Water, South England, filled the channel cross-section. The introduction of channel-spanning engineered logjams and increase in naturally formed logjams (Bennett et al., 2015; Burgess-Gamble et al., 2017; Gallisdorfer et al., 2014; Shields et al., 2004) are key components of river restoration and natural flood management projects (Roni et al., 2015). These projects must balance the benefits provided by LW (habitat creation and sediment retention) against the increase in flood risk. This tradeoff requires a robust method to predict the hydraulic impacts of LW jams and the implications on sediment transport and habitat, which are the goals of this paper.

To evaluate the hydraulic impact of LW jams, it is necessary to predict upstream water surface elevation, or backwater rise, from channel discharge and jam geometry (Dixon, 2016; Wohl et al., 2010). Backwater rise due to LW jams has previously been studied using empirical equations (Schalko et al., 2018, 2019; Schmocker & Hager, 2013). Shields and Gippel (1995) present a model to describe the energy loss due to LW based on the sum of flow resistance of individual logs. This approach becomes unwieldy for complex jams composed of many logs and for naturally occurring jams with unknown material properties (Manners et al., 2007). The lack of a predictive method for describing a jam's generation of backwater rise has been identified as a significant research gap preventing quantitative comparison of jams across river systems, standardized reporting of jam physical properties (Dixon, 2016; Scott et al., 2019; Wohl et al., 2010), and jam representation in numerical models (Hankin et al., 2020; Leakey et al., 2020; Persi et al., 2019; Ruiz Villanueva et al., 2014).

We present experimental results demonstrating that LW jams constructed of many logs, branches, and leaves can be modeled as a single porous structure, with loss of momentum within the jam described by the scale of individual solid elements and the number of elements per bed area, that is, an adaptation of the model for drag in canopies (Belcher et al., 2012; Finnigan, 2000; Nepf, 2012; Raupach, 1994). We show that the water depths at the upstream and downstream faces of the jam adjust to three constraints, illustrated in Figure 1, which then provide a prediction for the backwater rise:

1. Water surface drop through the jam $H_2 - H_3$ generates a net hydrostatic pressure force that balances the drag generated by jam elements.
2. Upstream water depth H_2 is minimized, which minimizes the total energy loss through the jam.

3. Water depth on the downstream face H_3 must be greater than or equal to the downstream water depth H_4. In many cases, $H_3 > H_4$, resulting in falling water on the downstream face of the jam.

With these constraints, the upstream water depth H_2 can be predicted from jam structural properties, discharge, channel width, and unobstructed water depth H_4. Based on this, a dimensionless parameter representing the structural properties of a jam is found from measurements of discharge, channel width, and unobstructed water depth H_4 and subsequently used to predict backwater rise under different discharge conditions.

2. Materials and Methods

The canopy drag model and prediction of upstream water depth were tested in 584 experiments that recorded water depths H_1 and H_4 1 m upstream and downstream of channel-spanning jams, respectively (Figure 1), for varying discharge $Q = 0.0026$ to 0.37 ($m^3\ s^{-1}$), flume width $B = 0.3$, 0.4, 1.5 (m), initial water depth $H_4 = 0.05$ to 0.44 (m), jam length $L = 0.05$ to 0.5 (m), LW diameter $d = 0.0023$ to 0.065 (m), and solid volume fraction $\phi = 0.17$ to 0.43 in smooth glass flumes. Solid volume fraction was found by dividing the measured solid wood volume by the measured jam volume (Schalko et al., 2018). Cylindrical logs were used to construct jams with logs held in place using either a rack of vertical metal rods or a set of thin acrylic plates attached to the flume sidewalls. The rack and plates were observed to have negligible effect on the water surface profile in tests with no LW present. A total of 214 cases measured the effect of imitation fir, natural willow, or natural fir branches added with the cylindrical logs. Volumetric discharge was measured by an electromagnetic flow meter. Flow adjustment at x_2 had no observable effect on the water surface profile, so that $H_1 \cong H_2$. H_4 was observed to equal the unobstructed water depth. Details of 548 experiments were previously published (Schalko et al., 2018). In these experiments H_1 and H_4 were measured using ultrasonic distance sensors. Flow depth was regulated by either varying flume slope between $S = 0 - 0.003$ in order to achieve the specified uniform flow depth H_4 (m) (Test Series A, Schalko et al., 2018) or controlled with a flap gate (Test Series B, Schalko et al., 2018), which produced gradually varied flow in a horizontal flume. Variation in water depth between H_1 and H_4 was within measurement error when no wood was present (Schalko et al., 2018). In addition, 36 experiments were conducted in an 0.3 (m) wide, 10 (m) long flume at Cardiff University (UK) with $S = 0.001$. For these cases H_1 and H_4 were measured using point gauges. For 203 experiments (36 tests performed at Cardiff University and selected experiments by Schalko et al., 2018), H_3 was measured with a ruler placed along the flume sidewall.

3. Development and Validation of Backwater Prediction

3.1. Adaptation of Canopy Drag Model

The canopy drag model was adapted to represent jams in the following way. A channel-spanning jam was assumed to be dynamically similar to an array of rigid cylindrical elements. Following the description used in canopy flows, the drag per fluid volume within the jam D_x ($N\ m^{-3}$) was represented by a quadratic drag law (Kaimal & Finnigan, 1994):

$$D_x = \frac{\rho C_D a}{2(1-\phi)} u^2, \tag{1}$$

in which the fluid density is ρ ($kg\ m^{-3}$) and u ($m\ s^{-1}$) is the time-averaged and spatially averaged longitudinal velocity. Because the drag acts on the fluid volume only, it was divided by the factor $(1-\phi)$. The solid volume fraction ϕ and spatially averaged frontal area per jam volume a (m^{-1}) are related by the geometry of jam elements. For jams composed of circular cylinders with diameter d, $\phi = \frac{\pi}{4} ad$ (Nepf, 2012). The drag coefficient $C_D = 0.9$ to 1.0 has been used for logs (Gippel et al., 1996), and here $C_D = 1$ was assumed throughout the analysis.

The validity of the canopy drag model (Equation 1) was demonstrated using a control volume between the upstream (x_2) and downstream (x_3) inner edges of a jam spanning a rectangular channel (Figure 1). Flow within the jam was assumed to be steady, one-dimensional, and incompressible, with momentum correction factor equal to 1 and hydrostatic pressure distribution. Frictional losses at the bed and sidewalls and

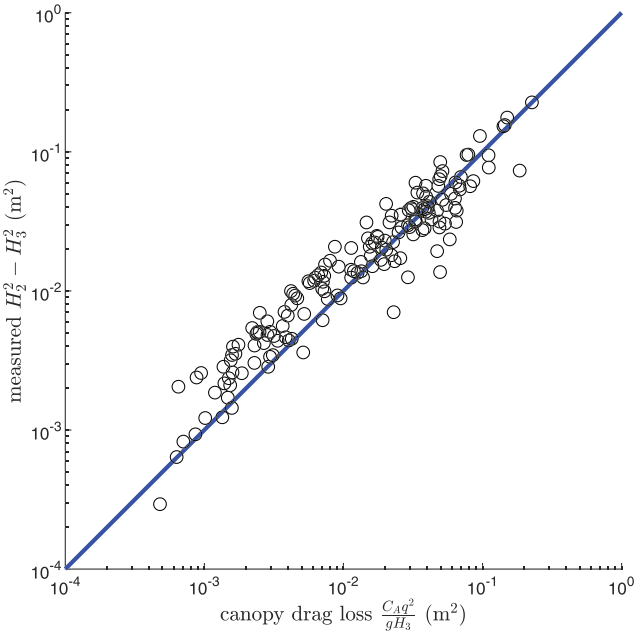

Figure 2. Measured change in square of water depth between x_2 and x_3 compared to canopy drag loss model with $C_D = 1.0$ (Equation 3; black open circles). Line of equality $y = x$ plotted in solid blue. Uncertainty in measurement of H_2 and H_3 was 0.001 m. Experiment reproducibility was evaluated by measuring repeat LW jams created with the same set of logs (Schalko et al., 2018). These measurements (17 sets of $n = 2$–3 repeats each) had standard error equal to 10% of the mean value. The difference $H_2^2 - H_3^2$ is linearly related to C_D, so variation of C_D by 10% (Gippel et al., 1996) yielded 10% difference in the result.

gravitational force due to weight of water on bed slope S were much smaller than frictional loss due to drag on logs. The integrated conservation of momentum for the control volume between x_2 and x_3 was then

$$\underbrace{\frac{1}{2}\rho g B(1-\phi)(H_2^2 - H_3^2)}_{\text{net hydrostatic pressure force}} + \underbrace{\rho B(1-\phi)(H_2 U_2^2 - H_3 U_3^2)}_{\text{net change in momentum}} - \underbrace{\frac{1}{2}\rho B L C_D a H_3 U_3^2}_{\text{drag within jam}} = 0, \quad (2)$$

with flow area at the upstream and downstream cross-sections $A_2 = BH_2(1-\phi)$, $A_3 = BH_3(1-\phi)$ (m^2), respectively, and spatially averaged longitudinal velocity $U = Q/[BH(1-\phi)]$ (m s^{-1}) inside the jam, with ϕ equal to the spatially averaged area fraction (Bluhm & de Boer, 1997). For the drag term, variation in water depth and velocity within the jam was approximated by the value at the downstream edge. Across all experimental conditions, net change in fluid momentum was on average 13% of the net hydrostatic pressure force term [95% confidence interval (CI) 6–39%]. For this reason, we neglected the second term in Equation 2. A dimensionless parameter was defined to represent jam geometry, $C_A = LC_D a/(1-\phi)^3$, and discharge per unit width of channel was defined as $q = Q/B$ (m^2 s^{-1}), such that Equation 2 becomes

$$H_2^2 - H_3^2 - \frac{C_A q^2}{g H_3} = 0. \quad (3)$$

The measured drop in water depth (specifically, $H_2^2 - H_3^2$) agreed with the value predicted from the canopy drag model (Equation 3) within uncertainty (Figure 2). The linear fit between measured $H_2^2 - H_3^2$ and $(C_A q^2)/(gH_3)$ had a slope 1.02 with 95% CI (0.98, 1.07) found from multiple linear regression (Matlab REGRESS).

Many pairs of (H_2, H_3) satisfy Equation 3. The additional constraint of minimum energy loss through the jam was used to isolate a single solution. The total energy loss ΔE_{24} between the jam upstream edge x_2 and the water depth measured 1 (m) downstream of the jam, at which the flow depth had recovered the unobstructed value (x_4), is

$$\Delta E_{24} = H_2 - H_4 - \frac{U_4^2}{2g}. \quad (4)$$

The magnitude of the velocity term at x_2, $U_2^2/2g$, was on average 1% of H_2 with 95% CI (0.4–3%) and was therefore neglected in Equation 4. Since H_4 was fixed by the existing downstream conditions, minimum energy loss was associated with the (H_2, H_3) pair corresponding to minimum H_2, found by solving Equation 3 for H_2 and finding $\partial H_2/\partial H_3 = 0$. This yielded

$$H_{3,\min} = \sqrt[3]{\frac{C_A q^2}{2g}}, \quad (5)$$

with subscript "min" used to define the solution with minimum energy. Applying Equation 5 in Equation 3, we find

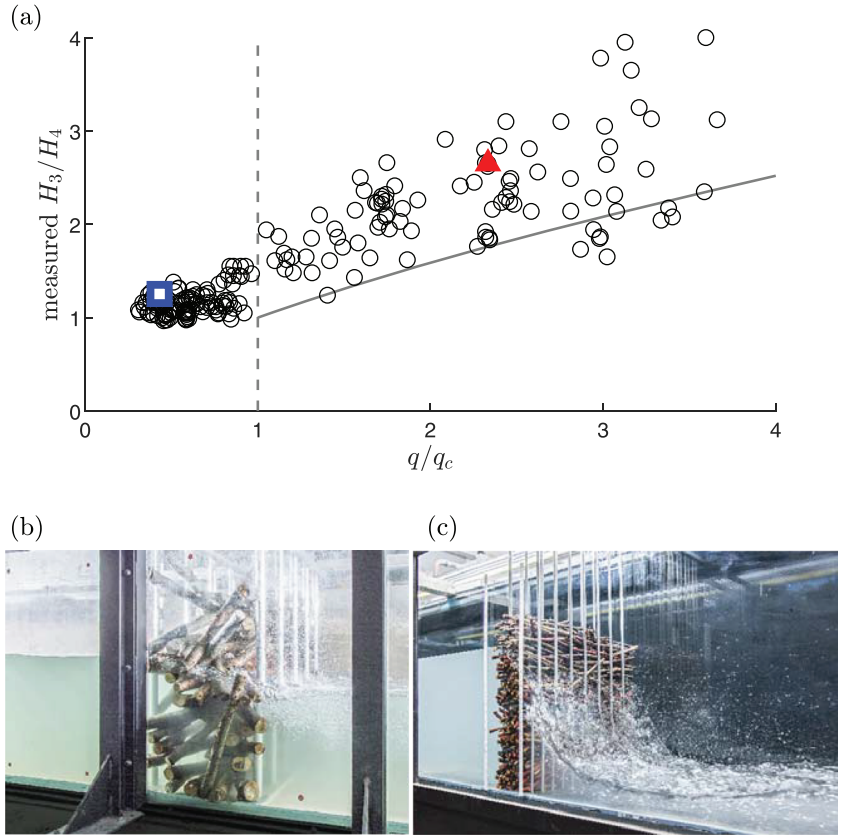

Figure 3. (a) Transition between cases with $H_3 = H_4$ and cases for which $H_3 > H_4$ (Equation 5). Black open circles show flume experiments with measured q, H_3, H_4, C_A. (b) Jam with $H_3 = H_4$ (Schalko et al., 2018, Test B26.5) corresponding to blue square in (a). (c) Jam with $H_3 > H_4$ (Schalko et al., 2018, Test A13.4) corresponding to red solid triangle in (a). Gray solid line ($y = x^{2/3}$) shows expected scaling for cases with predicted $H_{3,\min} > H_4$. Gray dashed line shows $q/q_c = 1$.

$$H_{2,\min} = \sqrt{3} H_{3,\min}. \tag{6}$$

In cases for which the predicted $H_{3,\min}$ (Equation 5) was greater than the downstream water depth H_4, falling water was observed on the back face of the jam (Figure 3c). While it is mathematically possible for the predicted $H_{3,\min}$ (Equation 5) to be less than H_4, this was never observed. When the predicted $H_{3,\min}$ was less than H_4, we observed $H_3 = H_4$, and no falling water was present on the back face of the jam (Figure 3b). That is,

$$H_{3,\min} = \max\left(H_4, \sqrt[3]{\frac{C_A q^2}{2g}}\right). \tag{7}$$

The corresponding $H_{2,\min}$ could then be found from Equation 3 with $H_{3,\min}$ given by Equation 7.

The transition between cases with ($H_3 > H_4$, Figure 3c) and without ($H_3 \cong H_4$, Figure 3b) falling water can be described by the condition $H_{3,\min} = H_4$, from which Equation 5 defines the critical unit discharge q_c at which falling water is initiated (i.e., $H_3 > H_4$),

$$q_c = \sqrt{\frac{2gH_4^3}{C_A}}. \tag{8}$$

The measurements supported this transition. Specifically, the data fell around $H_3/H_4 = 1$ for $q \le q_c$. For these cases the upstream water depth depended on the downstream (unobstructed) flow depth, as well as

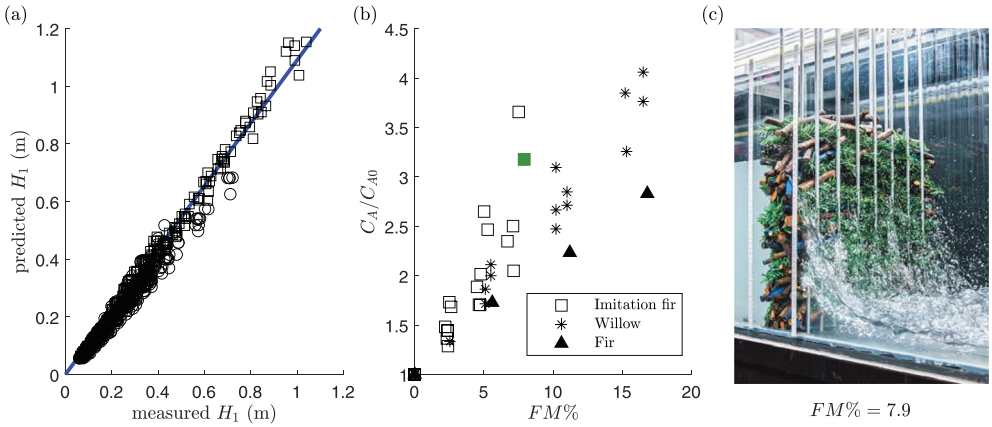

Figure 4. (a) Predicted and measured upstream water depth. Black open circles show prediction of H_1 for jams composed of logs only, with C_A predicted from measured L, d, ϕ. Black open squares show prediction for jams composed of logs and organic fine material FM, with C_A inferred from measurements of q, H_1, H_4 at the lowest q tested. Solid blue line shows $y = x$. (b) Increase in C_A with volume percentage of FM ($FM\%$) compared to $C_A = C_{A0}$ inferred for jams composed of logs only ($FM\% = 0$). Three types of FM were tested: imitation fir (black open squares), natural willow (black asterisks), and natural fir (black solid triangles). (c) Photo of jam composed of logs and imitation fir, with $FM\% = 7.9$ (Schalko et al., 2018, Test A62.3) corresponding to green solid square in (b).

q and C_A. For $q > q_c$, the depth ratio H_3/H_4 increased with $(q/q_c)^{2/3}$, following from Equation 5. For these conditions the upstream water depth depended only on q and C_A (Equation 6), and not the downstream flow condition. The canopy drag model could be used together with the minimum energy constraint to predict measured upstream water surface elevation H_1, which in our experiments was observed to equal H_2 within measurement error (Figure 4a). $H_1 \cong H_2$ was found from Equations 3 and 7. The linear fit between measured H_1 and predicted $H_1 \cong H_2$ had slope 0.95 with 95% CI (0.94, 0.96) found from multiple linear regression (Matlab REGRESS) (Figure 4a, black open circles).

4. Discussion

4.1. LW Jams Containing Organic Fine Material

The above analysis considered jams composed of groups of cylindrical logs, so that $a = 4\phi/\pi d$ (m^{-1}). In nature, jams may also contain organic fine material FM, providing additional blockage with noncylindrical elements (Manners et al., 2007). The effect of FM was tested experimentally (Schalko et al., 2018) through the addition of sets of imitation fir, natural willow, or natural fir branches to cylindrical logs (Figure 4b), with three to four discharge values measured for each jam. Structural complexity precluded calculation of a spatial average frontal area density, a, from material geometry. However, the dimensionless structural parameter C_A could be inferred from measurements of q, H_1, H_4. We used 214 sets of measurements (Schalko et al., 2018) with varying FM type and volume percentage ($FM\%$) to assess the validity of using C_A estimated from one discharge value to predict $H_1 \cong H_2$ for the same jam at a different discharge. C_A was found using Equation 3 with H_3 given by Equation 7 from measured q, H_1, H_4 at the lowest q tested. Then the inferred C_A was used to predict H_1 for each jam at all other tested discharge values. Predicted H_1 agreed with the measured value within uncertainty. Specifically, the prediction was, on average, 1.05 ± 0.13 (95% CI) times the measured value (Figure 4a, black open squares). This confirmed that the above approach could be used to deduce C_A from measurements recorded at low discharge levels (which occur most frequently) and then to predict H_1 at other discharge values for preexisting LW jams containing FM, similar to naturally occurring jams.

The presence of FM increased C_A relative to $C_A = C_{A0}$ obtained with only logs present (Figure 4b). C_A increased approximately linearly with increasing $FM\%$ added. The relative increase of C_A/C_{A0} had slopes (95% CI; Matlab REGRESS) equal to 0.23 (0.2, 0.26), 0.17 (0.16, 0.18), and 0.11 (0.1, 0.12) with $R^2 = 0.83$, 0.97, 0.99 for imitation fir, natural willow, and natural fir branches, respectively. Relative rate of C_A increase

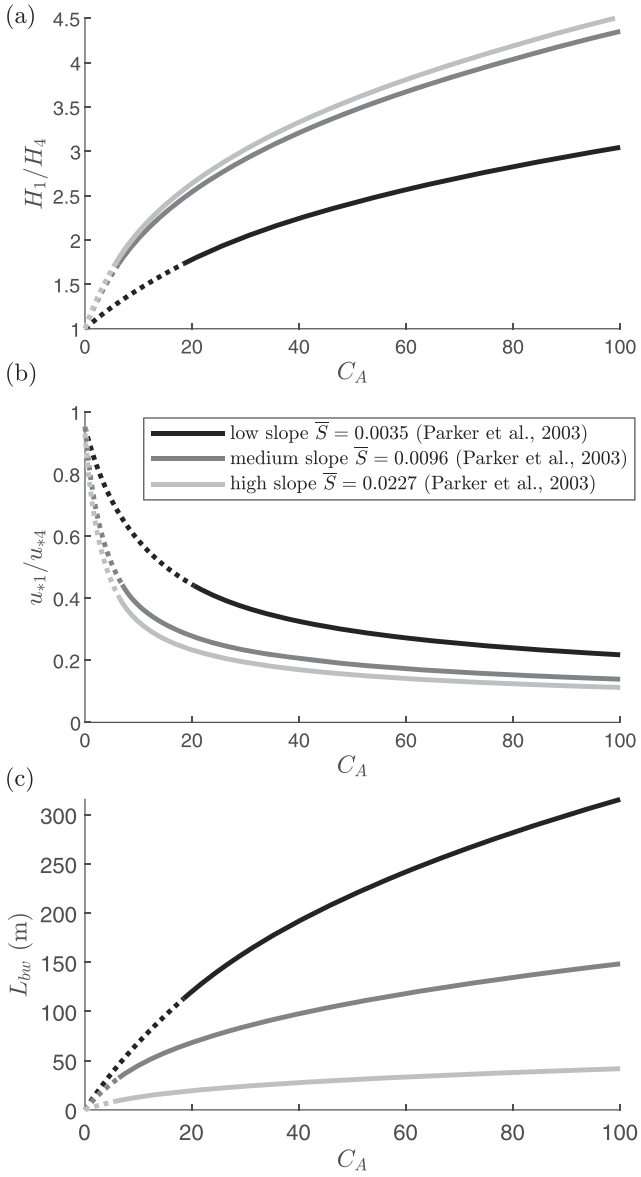

Figure 5. Change in (a) relative backwater rise H_1/H_4 (Equations S1a and S1b), (b) relative bed shear velocity u_{*1}/u_{*4} (Equations S2a and S2b), and (c) estimated backwater length L_{bw} with $C_A = 1$–100 for streams with $H_4 = 0.5H_{bf}$, B_{bf}, d_{s50}, S equal to average properties observed for groups of low, medium, and high slope streams (black, gray, and light gray lines; Parker et al., 2003). Jams without ($H_3 \cong H_4$) and with ($H_3 > H_4$) falling water at the jam downstream edge are shown respectively with dashed and solid lines.

was much greater than change in ϕ. For example, an addition of willow branches that increased ϕ by 16.5% increased C_A by 406%. Together with the observed linear trend, this indicated that addition of *FM* primarily increased a at a rate dependent on *FM* size and shape. This is consistent with the relationship $a = 4\phi/\pi d$ for cylinders and $a \sim \phi/L_v$ for other shapes with characteristic length scale L_v. Because the characteristic length scale of *FM* was much smaller than d (Figure 4c), a given increase in ϕ due to *FM* addition resulted in a much larger increase in a, compared to the same ϕ increase achieved by addition of logs. In addition to the effect of size alone, *FM* contained noncylindrical material, which had a higher surface area to volume ratio relative to cylindrical logs.

4.2. Spatial Extent of Backwater Rise Upstream of LW Jam and Impact on Sediment Transport

Jams induce an increase in water depth extending over some distance upstream, which in turn reduces channel velocity and sediment transport capacity, promoting sediment deposition in the upstream region. The new jam model was used to explore the spatial extent of backwater rise and associated decrease in sediment transport capacity, reflected in the reduction in bed shear velocity, $u_* = \sqrt{C_f}U$ (see supporting information). Specifically, both suspended and bedload transport decrease with decreasing u_*, with suspended transport related to the ratio of u_* to sediment settling velocity w_s and bedload transport related to bed shear stress $\tau_b = \rho u_*^2$ (Julien, 1998; Yang & Nepf, 2018). The increase in backwater rise and associated reduction in u_* reduce sediment transport over backwater length L_{bw}, a reach extending approximately from the jam upstream edge to the point at which the stream depth is equal to the unobstructed uniform flow depth (H_4). A transition between jams without ($H_3 \cong H_4$) and with ($H_3 > H_4$) falling water on the downstream face of the jam (Figure 3) occurred at $(C_A S)/C_{f4} = 2$ (Figure 5, dashed and solid lines, respectively). The relative magnitude of backwater rise and associated reduction in u_* increased with increasing C_A (Figures 5a and 5b). Because the uniform flow depth scales inversely with S ($H_4 \sim S^{-1/3}$), the ratios of water depth and bed shear velocity (H_1/H_4, u_{*1}/u_{*4}) deviated further from 1 with increased S for a given C_A (Figures 5a and 5b). For example, a jam with $C_A = 40$ generated a backwater rise of ≈3 times the uniform flow depth for high and medium slope streams (Figure 5a, gray and light gray lines), but only ≈2 times the uniform flow depth for low slope streams (Figure 5a, black line). Therefore, a given jam in a high slope stream creates a larger backwater rise and increased sediment deposition due to a decreased friction velocity. The estimated backwater length L_{bw} increased from zero to between 40 and 300 m for $C_A = 0$ to 100, depending on stream characteristics (Figure 5c). This was in agreement with field observations that jams increase sediment retention upstream of a jam over an upstream reach extending from 10^1 to 10^2 m (Wohl & Scott, 2017). The estimated backwater length L_{bw} (Figure 5c) and associated backwater pool volume $V_{\text{pool}} = L_{bw} B(H_1 - H_4)$ increased with increasing C_A and decreasing S, which was consistent with a meta-analysis (Wohl & Scott, 2017) of field observations that pool volume correlates negatively with slope and positively with LW volume.

5. Conclusions

Recent recognition of the geomorphic and ecological role of LW (Collins et al., 2012; Walter & Merritts, 2008; Wohl, 2017) has led to an increase in wood reintroduction and engineered logjam installation efforts in order to promote the hydroecological benefits associated with LW, which is a shift in perspective from historic LW removal and stream channelization efforts (Burgess-Gamble et al., 2017; Gurnell et al., 2018; Wohl, 2017). Prediction of the upstream backwater rise generated by channel-spanning LW jams is necessary in order to understand jam effects on sediment transport and ecological processes, to compare LW jams across river systems, and to represent LW jams in hydraulic modeling frameworks. In this paper momentum and energy constraints were combined to predict the backwater rise generated by channel-spanning LW jams composed of many logs and branches with needles and leaves (Equations 3–7). Backwater rise was dependent on unit discharge q, unobstructed water depth H_4, and a dimensionless parameter C_A, which may be inferred from measurements of q, H_1, H_4. Based on this new approach, we determined the spatial extent of the backwater rise and explored the decrease in sediment transport capacity for a LW jam in low, medium, and high slope streams (Parker et al., 2003). This approach allows quantification of the physical role of LW jams in generating geomorphic and ecological diversity and stabilizing channel networks (Collins et al., 2012; Walter & Merritts, 2008). C_A could be used to characterize physical properties of preexisting LW jams (Dixon, 2016; Wohl et al., 2010) and compare LW jams across river systems through collaborative LW data collection (Scott et al., 2019). C_A may also be predicted from LW jam length, solid volume fraction, and log diameter, allowing representation of engineered logjam designs in a flood model or network analysis (Hankin et al., 2020; Leakey et al., 2020; Persi et al., 2019; Ruiz Villanueva et al., 2014) as a composite structure (Equations 3 and 7). This may improve the design and long-term assessment of engineered logjams used in river restoration and natural flood management. The predicted spatial impact of jams on backwater length and generated pool size were consistent with field observations.

Data Availability Statement

Data sets for this research are available in Schalko (2018) and Follett (2019) (CC BY 4.0).

Acknowledgments

The first author has received funding from the European Union's Horizon 2020 research and innovation program under the Marie Skłowdowska-Curie grant agreement WoodJam No. 745348, and the second author is funded by the Swiss National Science Foundation (SNSF) (Early Postdoc Mobility Fellowship; Project 184263).

References

Abbe, T., & Montgomery, D. (2003). Patterns and processes of wood debris accumulation in the Queets river basin, WA. *Geomorphology*, *51*, 81–107. https://doi.org/10.1016/S0169-555X(02)00326-4

Beckman, N., & Wohl, E. (2014). Carbon storage in mountainous headwater streams: The role of old-growth forest and logjams. *Water Resources Research*, *50*, 2376–2393. https://doi.org/10.1002/2013WR014167

Belcher, S., Harman, I., & Finnigan, J. (2012). The wind in the willows: Flows in forest canopies in complex terrain. *Annual Review of Fluid Mechanics*, *44*, 479–504. https://doi.org/10.1146/annurev-fluid-120710-101036

Bennett, S., Ghaneeziad, S., Gallisdorfer, M., Cai, D., Atkinson, J., Simon, A., & Langendoen, E. (2015). Flow, turbulence and drag associated with engineered log jams in a fixed-bed experimental channel. *Geomorphology*, *248*, 172–184. https://doi.org/10.1016/j.geomorph.2015.07.046

Bertoldi, W., Welber, M., Gurnell, A., Mao, L., Comiti, F., & Tal, M. (2015). Physical modelling of the combined effect of vegetation and wood on river morphology. *Geomorphology*, *246*, 178–187. https://doi.org/10.1016/j.geomorph.2015.05.038

Bezzola, G., & Hegg, C. (2007). Ereignisanalyse hochwasser 2005 teil 1: Prozesse, schäden und erste einordnung [Analysis of 2005 flood event. 1: Processes, damages and classification] (*Report*): Bern, Switzerland Federal Office for the Environment FOEN, Swiss Federal Institute for Forest, Snow, and Landscape Research WSL. In German. Available: https://www.dora.lib4ri.ch/wsl/islandora/object/wsl:10508

Bluhm, J., & de Boer, R. (1997). The volume fraction concept in the porous media theory. *Journal of Applied Mathematics and Mechanics*, *77*, 563–577. https://doi.org/10.1002/zamm.19970770803

Burgess-Gamble, L., Ngai, R., Wilkinson, M., Nisbet, T., Pontee, N., Harvey, R., et al. (2017). Working with natural processes - evidence directory (Technical Report No. SC150005). Horizon House, Deanery Road, Bristol, BS1 5AH Environment Agency.

Collins, B., Montgomery, D., Fetherston, K., & Abbe, T. (2012). The floodplain large-wood cycle hypothesis: A mechanism for the physical and biotic structuring of temperate forested alluvial valleys in the North Pacific coastal ecoregion. *Geomorphology*, *139-140*, 460–470. https://doi.org/10.1016/j.geomorph.2011.11.011

Comiti, F., Lucía, A., & Rickenmann, D. (2016). Large wood recruitment and transport during large floods: A review. *Geomorphology*, *269*, 23–39. https://doi.org/10.1016/j.geomorph.2016.06.016

De Cicco, P. j. E. P., Ruiz-Villanueva, V., Solari, L., & Stoffel, M. (2017). In-channel wood-related hazards at bridges: A review. *River Research and Applications*, *34*, 617–628. https://doi.org/10.1002/rra.3300

Dixon, S. (2016). A dimensionless statistical analysis of logjam form and process. *Ecohydrology*, *9*, 1117–1129. https://doi.org/10.1002/eco.1710

Entrekin, S., Tank, J., Rosi-Marshall, E., Hoellein, T., & Lamberti, G. (2008). Responses in organic matter accumulation and processing to an experimental wood addition in three headwater streams. *Freshwater Biology*, *53*, 1642–1657. https://doi.org/10.1111/j.1365-2427.2008.01984.x

Finnigan, J. (2000). Turbulence in plant canopies. *Annual Review of Fluid Mechanics*, *32*, 519–571. https://doi.org/10.1146/annurev.fluid.32.1.519

Follett, E. (2019). *Dataset: Backwater rise due to wood accumulations in experimental flume*: Zenodo. Accessed 2020-08-01. https://doi.org/10.5281/zenodo.3968568

Gallisdorfer, M., Bennett, S., Atkinson, J., Ghaneeizad, S., Brooks, A., Simon, A., & Langendoen, E. (2014). Physical-scale model designs for engineered log jam in rivers. *Journal of Hydro-environment Research*, *8*, 115–128. https://doi.org/10.1016/j.jher.2013.10.002

Gippel, C. (1995). Environmental hydraulics of large woody debris in streams and rivers. *Journal of Environmental Engineering*, *121*, 388–395. https://doi.org/10.1061/(ASCE)0733-9372(1995)121:5(388)

Gippel, C., O'Neill, I., Finlayson, B., & Schnatz, I. (1996). Hydraulic guidelines for the reintroduction and management of large woody debris in lowland rivers. *Regulated Rivers: Research & Management*, *12*, 223–236. https://doi.org/10.1002/(SICI)1099-1646(199603)12:2/3<223::AID-RRR391>3.0.CO;2-%23

Gurnell, A., England, J., & Burgess-Gamble, L. (2018). Trees and wood: Working with natural river processes. *Water and Environment Journal*, *33*, 342–352. https://doi.org/10.1111/wej.12426

Hankin, B., Hewitt, I., Sander, G., Danieli, F., Formetta, G., Kamilova, A., et al. (2020). A risk-based, network analysis of distributed in-stream leaky barriers for flood risk management. *Natural Hazards and Earth System Sciences*. https://doi.org/10.5194/nhess-2019-394

Haschenburger, J., & Rice, S. (2004). Changes in woody debris and bed material texture in a gravel-bed channel. *Geomorphology*, *60*, 241–267. https://doi.org/10.1016/j-geomorph.2003.08.003

Julien, P. (1998). *Erosion and sedimentation*. Cambridge, UK: Cambridge University Press.

Kaimal, J., & Finnigan, J. (1994). *Atmospheric boundary layer flows: Their structure and measurement*. New York, New York: Oxford University Press.

Keller, E., & Swanson, F. (1979). Effects of large organic material on channel form and fluvial processes. *Earth Surface Processes and Landforms*, *4*, 361–380. https://doi.org/10.1002/esp.3290040406

Leakey, S., Hewett, C., Glenis, V., & Quinn, P. (2020). Modelling the impact of leaky barriers with a 1D Godunov-type scheme for the shallow water equations. *Water*, *12*, 371. https://doi.org/10.3390/w12020371

Manners, R., Doyle, M., & Small, M. (2007). Structure and hydraulics of natural woody debris jams. *Water Resources Research*, *43*, W06432. https://doi.org/10.1029/2006WR004910

Nepf, H. (2012). Flow and transport in regions with aquatic vegetation. *Annual Review of Fluid Mechanics*, *44*, 123–142. https://doi.org/10.1146/annurev-fluid-120710-101048

Panici, D., & de Almeida, G. (2018). Formation, growth, and failure of debris jams at bridge piers. *Water Resources Research*, *54*, 6226–6241. https://doi.org/10.1029/2017WR022177

Parker, G., Toro-Escobar, C., Ramey, M., & Beck, S. (2003). Effect of floodwater extraction on mountain stream morphology. *Journal of Hydraulic Engineering*, *129*, 885–895. https://doi.org/10.1061/(ASCE)0733-9429(2003)129:11(885)

Persi, E., Petaccia, G., Sibilla, S., Lucıa, A., Andreoli, A., & Comiti, F. (2019). Numerical modelling of uncongested wood transport in the Rienz river. *Environmental Fluid Mechanics*, *20*, 539–558. https://doi.org/10.1007/s10652-019-09707-8

Raupach, M. (1994). Simplified expressions for vegetation roughness length and zero-plane displacement as functions of canopy height and area index. *Boundary-Layer Meteorology*, *71*, 211–216. https://doi.org/10.1007/BF00709229

Roni, P., Beechie, T., & Pess, G. (2015). Wood placement in river restoration: Fact, fiction, and future direction. *Canadian Journal of Fisheries and Aquatic Sciences*, *72*, 46–478. https://doi.org/10.1139/cjfas-2014-0344

Ruiz Villanueva, V., Castellet, E., Díez-Herrero, A., Bodoque, J., & Sánchez-Juny, M. (2014). Two-dimensional modelling of large wood transport during flash floods. *Earth Surface Processes and Landforms*, *39*, 438–449. https://doi.org/10.1002/esp.3456

Schalko, I. (2018). *Dataset: Backwater rise due to large wood accumulations*: Zenodo. Accessed 2020-08-01 https://doi.org/10.5281/zenodo.2640932

Schalko, I., Lageder, C., Schmocker, L., Weitbrecht, V., & Boes, R. (2019). Laboratory flume experiments on the formation of spanwise large wood accumulations part I: Effect on backwater rise. *Water Resources Research*, *55*, 4854–4870. https://doi.org/10.1029/2018WR024649

Schalko, I., Schmocker, L., Weitbrecht, V., & Boes, R. (2018). Backwater rise due to large wood accumulations. *Journal of Hydraulic Engineering*, *144*, 04018056. https://doi.org/10.1061/(ASCE)HY.1943-7900.0001501

Schmocker, L., & Hager, W. (2013). Scale modeling of wooden debris accumulation at a debris rack. *Journal of Hydraulic Engineering*, *139*, 827–836. https://doi.org/10.1061/(ASCE)HY.19437900.0000714

Scott, D., Wohl, E., & Yochum, S. (2019). Wood Jam Dynamics Database and Assessment Model (WooDDAM): A framework to measure and understand wood jam characteristics and dynamics. *River Research and Applications*, *35*, 1466–1477. https://doi.org/10.1002/rra.3481

Shields, F., & Gippel, C. (1995). Prediction of the effect of woody debris removal on flow resistance. *Journal of Hydraulic Engineering*, *121*, 341–354. https://doi.org/10.1061/(ASCE)0733-9429(1995)121:4(341)

Shields, F., Morin, N., & Cooper, C. (2004). Large woody debris structures for sand-bed channels. *Journal of Hydraulic Engineering*, *130*, 208–217. https://doi.org/10.1061/(ASCE)0733-9429(2004)130:3(208)

Steeb, N., Rickenmann, D., Badoux, A., Rickli, C., & Waldner, P. (2017). Large wood recruitment processes and transported volumes in Swiss mountain streams during the extreme flood of August 2005. *Geomorphology*, *279*, 112–127. https://doi.org/10.1016/j.geomorph.2016.10.011

Wallerstein, N., Alonso, C., Bennett, S., & Thorne, C. (2001). Distorted Froude-scale flume analysis of large woody debris. *Earth Surface Processes and Landforms*, *26*, 1265–1283. https://doi.org/10.1002/esp.271

Walter, R., & Merritts, D. (2008). Natural streams and the legacy of water-powered mills. *Science*, *319*, 299–304. https://doi.org/10.1126/science.1151716

Wohl, E. (2017). Bridging the gaps: An overview of wood across time and space in diverse rivers. *Geomorphology*, *279*, 3–26. https://doi.org/10.1016/j.geomorph.2016.04.014

Wohl, E., Bledsoe, B., Fausch, K., Kramer, N., Bestgen, K., & Gooseff, M. (2016). Management of large wood in streams: An overview and proposed framework for hazard evaluation. *Journal of the American Water Resources Association*, *52*, 315–335. https://doi.org/10.1016/j.geomorph.2016.04.014

Wohl, E., Cenderelli, D., Dwire, K., Ryan-Burkett, S., Young, M., & Fausch, K. (2010). Large in-stream wood studies: A call for common metrics. *Earth Surface Processes and Landforms*, *35*, 618–625. https://doi.org/10.1002/esp.1966

Wohl, E., & Goode, J. (2008). Wood dynamics in headwater streams of the Colorado Rocky Mountains. *Water Resources Research*, *44*, W09429. https://doi.org/10.1029/2007WR006522

Wohl, E., & Jaeger, K. (2009). A conceptual model for the longitudinal distribution of wood in mountain streams. *Earth Surface Processes and Landforms*, *34*, 329–344. https://doi.org/10.1002/esp.1722

Wohl, E., & Scott, D. (2017). Wood and sediment storage and dynamics in river corridors. *Earth Surface Processes and Landforms*, *42*, 5–23. https://doi.org/10.1002/esp.3909

Yang, J., & Nepf, H. (2018). A turbulence-based bed-load transport model for bare and vegetated channels. *Geophysical Research Letters*, *45*, 10,428–10,436. https://doi.org/10.1029/2018GL079319